JOURNAL OF SPACECRAFT AND ROCKETS
Vol. 31, No. 5, September–October 1994

Hypersonic Nonequilibrium Navier-Stokes Solutions over an Ablating Graphite Nosetip

Y.-K. Chen* and W. D. Henline†
NASA Ames Research Center, Moffett Field, California 94035

The general boundary conditions, including mass and energy balances, of chemically equilibrated or nonequilibrated gas adjacent to ablating surfaces have been derived. A computer procedure based on these conditions was developed and interfaced with the Navier-Stokes solver GASP (General Aerodynamics Simulation Program). A test case with a proposed hypersonic test-vehicle configuration and associated freestream conditions was developed. The solutions of the GASP code with various surface boundary conditions were obtained and compared with those of the ASCC (ABRES Shape Change) code, and the effect of nonequilibrium gas as well as surface chemistry on surface heating and ablation rate were examined.

Nomenclature

A = area, m^2
B' = quantity defined in Eq. (7)
C_H = H-type heat-transfer coefficient, kg/m^2 · s
C_M = mass-transfer coefficient
C_T = T-type heat-transfer coefficient, J/m^2 · s · K
C_p = specific heat, J/kg · K
D = diffusion coefficient, m^2/s
H_r = recovery enthalpy, J/kg
h = enthalpy, J/kg
J_v = net mass flux leaving surface, kg/m^2 · s
K = elemental-mass fraction
k = Boltzmann constant, J/K
k_t = thermal conductivity, W/m · K
m = species mass, kg
m_b = normalized surface blowing rate, $(\rho v)_w/(\rho v)_\infty$
N_k = total number of elements
N_s = total number of species
N_r = total number of surface reactions
P = pressure, N/m^2
P_v = saturated vapor pressure, N/m^2
q = heat flux, W/m^2
q_c = convective surface heat flux, W/m^2
q_{rad} = radiative heat flux, W/m^2
q_{cond} = conductive heat flux, W/m^2
R_e = Reynolds number
R_n = nose radius of blunt body, m
T = temperature, K
T_r = recovery temperature, K
U = velocity, m/s
v = velocity component normal to surface, m/s
x = species mass fraction
$\tilde{Z}_k^*$ = weighted average of the mole and mass fractions
ϵ = surface emissivity
η = coordinate normal to surface, m
ρ = density, kg/m^3
σ = Stefan-Boltzmann constant, W/m^2 · K^4
σ_v = evaporation coefficient
ω = mass flux due to surface chemical reaction, kg/m^2 · s

Subscripts
e = outer edge of boundary layer
i = species
k = element
s = solid
w = wall
∞ = freestream

Received May 18, 1993; revision received Jan. 24, 1994; accepted for publication Jan. 25, 1994.

*Research Scientist, Thermosciences Institute, MS 234-1. Member AIAA.
†Research Scientist, Thermal Protection Materials Branch. Senior Member AIAA.

Introduction

In recent years, computational fluid-dynamics (CFD) technology has continued to develop in the areas of nonequilibrium flow, multispecies kinetics and transport properties, and multidimensional full Navier-Stokes capabilities. However, most codes use primitive surface boundary conditions and cannot be realistically used to predict the aerothermal heating for the design of thermal protection systems (TPS). The general boundary conditions should include appropriate energy and multispecies mass balances with surface-kinetics models and surface ablation.[1]

For aerothermal heating predictions over nonablating TPS, some efforts have been made to determine catalytic coefficients[2–4] and demonstrate the importance of surface catalysis, nonequilibrium kinetics, and multispecies transport properties for the prediction of aerothermal heating. Surface energy and mass balances with surface catalytic reactions have been incorporated into state-of-the-art Navier-Stokes codes.[5,6]

For aerothermal heating predictions over ablating TPS, some CFD codes were developed with surface mass and energy balances. The BLIMPK code[7] is a two-dimensional ablating boundary-layer code with multispecies transport and chemical equilibrium or nonequilibrium chemistry for both the gas and the surface. Because of the nature of boundary-layer equations, the boundary-layer edge properties must be provided in the calculations. The determination of edge properties, especially for a chemically nonequilibrium edge in a non-Newtonian flow, is usually a stumbling block in using BLIMPK to simulate flows over high-angle blunt bodies. The HYVIS[8] and RASLE[9] codes were developed for the analysis of axisymmetric radiating viscous shock layers. In the HYVIS code, a sublimation surface temperature is applied in its surface energy balance. The RASLE code can solve the surface energy and mass-balance equations to compute the ablation flux and wall temperature as part of its solution. Due to the nature of the parabolized formulation in the HYVIS and RASLE codes, full forebody solutions over a high-angle blunt body can be obtained only for some special cases. Both codes are commonly used for determining approximate solutions for flow coupled with radiation along the stagnation streamline. Bhutta and Lewis developed a PNS code[10] with finite-rate gas chemistry, constant surface temperature, and equilibrium surface species concentrations. Initial conditions to start these PNS calculations must be generated by a VSL or full Navier-Stokes code. Recently, Conti et

al. computed an axisymmetric Navier-Stokes solution with carbon ablation and shape change[11] but with no chemical reactions between ablated carbon and air. Only an incomplete set of surface boundary conditions was employed.

Although considerable uncertainties remain in multispecies transport coefficients and chemical-kinetics models, the use of multispecies and multidimensional full Navier-Stokes calculations has been common practice in the CFD community. A large-angle blunt body is a common configuration to which such codes are applied. Because of the large subsonic region in a blunt-body shock layer, the flowfield and aerothermal heating in such case cannot be precisely predicted without the full Navier-Stokes calculation. However, none of the available Navier-Stokes solvers include complete boundary conditions to realistically determine aerothermal heating and surface ablation rates. In this study, a general surface boundary condition including energy and mass balances with the surface thermochemistry effects is developed for nonequilibrium or equilibrium gas states adjacent to an ablating or nonablating surface. Based on this formulation, a surface thermochemistry computer procedure is developed and interfaced with available Navier-Stokes codes. Thus, a wider range of flow conditions can then be simulated. Radiation and turbulent effects may be important in an ablating flowfield; however, they are not included in this paper. A flow chart in Fig. 1 presents the relationship among computational surface thermochemistry (CST), computational fluid dynamics (CFD), and computational solid mechanics (CSM) codes. The interface between the CST and CSM codes for the prediction of in-depth conduction and shape change is also not included, i.e., the flowfield and solid calculations are not coupled.

A test case using a proposed hypersonic test-vehicle configuration and associated freestream conditions is developed in this paper. This test vehicle has a graphite nosetip with a radius R_n of 0.0176 m and a cone half angle of 6.5 deg. The multispecies Navier-Stokes equations were solved using GASP.[12] The surface ablation rates over the nosetip predicted by the GASP code with the present CST procedure are compared with the available solutions of the ASCC[13] code. In the ASCC code, in-depth conduction and shape change are properly considered with complete surface energy-balance equations. These features are not included in any available shock-layer or boundary-layer codes. This makes it possible to perform time-dependent calculations along the entire trajectory. The ASCC code has been widely applied to predicting carbon ablation rates over reentry vehicles with small nosetips.[14] The flowfield calculations in the ASCC code are approximated by the momentum energy integral technique (MEIT).[13,14] Heat- and mass-transfer coefficients are obtained by solving the global integral boundary-layer equations of an ideal gas with semiempirical correlations to account for real-gas, surface roughness, turbulence, and high-altitude effects. The detailed flowfield and gas species migration cannot be obtained in the ASCC calculations. So far there are no solutions for flow over a large-angle blunt body with ablating surface available for comparison. Thus, this test case is to check the code consistency and identify sensitive areas in the algorithm, but not to fully explore the capability of full Navier-Stokes calculations, e.g., as represented by a complete solution for flow over a large-angle blunt body.

Surface Boundary Conditions

The schematic diagram depicting the energy and species mass fluxes in a gas adjacent to a surface is shown in Fig. 2. The general boundary conditions for a chemically nonequilibriated, noncharring ablating surface can be written as

$$\rho D_i \left.\frac{\partial x_i}{\partial \eta}\right|_w + J_v x_{is} = \rho v x_i + \sum_{r=1}^{N_r} \omega_i^r \qquad (i = 1, \ldots, N_s) \quad (1)$$

$$k_t \frac{\partial T_w}{\partial \eta} + \sum_{i=1}^{N_s} h_i \rho D_i \left.\frac{\partial x_i}{\partial \eta}\right|_w + q_{\text{rad}}$$

$$= \rho v h_w - J_v h_s + \varepsilon \sigma T_w^4 + q_{\text{cond}} \quad (2)$$

$$J_v = J_v^{\text{evap}} - J_v^{\text{recond}} = \rho v \quad (3)$$

Here, the net mass flux leaving the surface, J_v, can be determined by the kinetic theory or correlations[15,16]; the mass flux of species i consumed by surface reaction r, ω_i^r, can be predicted based on surface-kinetics models. For charring TPS materials, additional terms with pyrolysis gas flux have to be considered in the above boundary conditions. Equations (1) and (2) can also be applied on the nonablating surfaces, if J_v and ρv are set to zero.[5,6]

If the gas adjacent to the surface is in a state of chemical nonequilibrium, the surface ablating rates, species concentrations, and temperature can be predicted from Eqs. (1–3) with appropriate thermodynamic and transport properties. However, for those TPS materials whose surface and associated gas reaction-rate data are not available, this kind of nonequilibrium analysis is probably not justified. In this case, some kind of approximation technique is more appropriate.

If the diffusion coefficients of all species are assumed to be equal, then a summation of the species mass-balance equation (1) yields a balance equation for each element k, and consequently eliminates the surface reaction term:

$$\rho D \left.\frac{\partial K_k}{\partial \eta}\right|_w + J_v K_{ks} = \rho v K_k \qquad (k = 1, \ldots, N_k) \quad (4)$$

Here, N_k is the total number of elements. By definition the following correlation for a dimensionless mass-transfer coefficient C_M exists for the elements k:

$$C_M = \frac{\rho D}{\rho_e u_e (K_{ke} - K_k)} \left.\frac{\partial K_k}{\partial \eta}\right|_w \qquad (k = 1, \ldots, N_k) \quad (5)$$

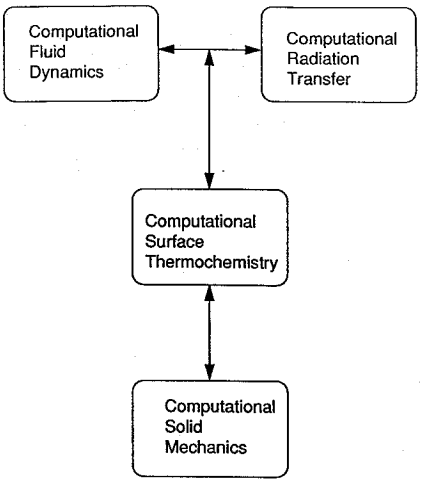

Fig. 1 Flow chart for computational surface thermochemistry.

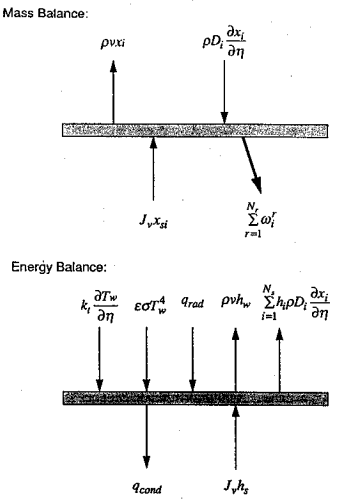

Fig. 2 Surface mass and energy balances.

and substituting Eq. (5) into Eq. (4), the elemental balance equation becomes

$$K_{ke} + B'K_{ks} = (1 + B')K_k \tag{6}$$

In Eq. (6), the dimensionless parameter B' for the surface ablation rate[17] is adopted:

$$B' = \frac{J_v}{\rho_e u_e C_M} \tag{7}$$

These relations can still be used in modified form for unequal diffusion coefficients for all species; i.e., instead of Eq. (5), C_M is now represented as

$$C_M = \frac{\rho D}{\rho_e u_e (\tilde{Z}^*_{ke} - \tilde{Z}^*_k)} \frac{\partial K_k}{\partial \eta}\bigg|_w \tag{8}$$

Here $\tilde{Z}^*_k$ is a weighted average of the mole and mass fractions ot element k, and its definition is presented in Ref. 17. For a surface in chemical equilibrium, the chemical and thermodynamic states of the gas can be fully determined from equilibrium relations based on the elemental species concentrations, temperature, pressure, and equilibrium constants. With Eq. (6) and equilibrium conditions, the value of B' can be determined for a given set of surface temperatures and pressures.[17] In this situation, surface ablation rates can be estimated without the knowledge of detailed surface kinetics and kinetic theory. Therefore, the net surface ablation rate is equal to

$$J_v = B'(T_w, P_w)C_M \tag{9}$$

Here the ablation rate is expressed as a function of B' and mass diffusion rate. The diffusion coefficient then plays a dominant role in determining the surface ablation rate.[18] The species concentrations are calculated from Eq. (6) and equilibrium relations, and the surface temperature is determined from the surface energy balance, Eq. (2).

Computational Method

A CST procedure was developed, based on the equations discussed in the previous section. This procedure is designed to be interfaced with Navier-Stokes solvers, such as GASP, to explicitly update the surface thermochemical properties and boundary conditions for ablating or nonablating surfaces. The final goal of this work is to develop a general-purpose procedure ready to be interfaced with various CFD tools, with minimum possible CFD code modifications for TPS design. A general implicit scheme for inclusion of boundary conditions may somewhat improve the CPU time for some cases; however, it requires much more CFD code modification and makes the development of a general-purpose procedure capable of interfacing with various codes unwieldy. From our experience with BLIMPK, it was an extremely lengthy and frustrating process to obtain a proper initial guess to start the calculation with fully implicit ablating CST conditions. Thus, BLIMPK has been modified, according to the idea discussed in this study, to perform global iterations and explicitly update the surface temperature for predicting the surface heating and ablation rates over the Apollo lunar/earth return capsule.[19] Without a global iteration scheme, BLIMPK solutions with complete implicit ablation boundary conditions were extremely difficult to obtain.

The first two terms in Eq. (2) are the convective heat flux (q_c,w) to the surface and are obtained from the CFD solutions. Equation (2) can be written as

$$q_{c,w(\mathrm{CFD})} + q_{\mathrm{rad}} = \rho v h_w - J_v h_s + \varepsilon\sigma T_w^4 + q_{\mathrm{cond}} \tag{10a}$$

The new surface temperature of the next global iteration can be directly obtained from the solution of Eq. (10a). However, for space vehicles with significant in-depth conduction (q_{cond}), or strong temperature gradients along the surface, a simple, fully explicit method may not be adequate. From our experience, using the local value of the convective heat-transfer coefficient in Eq. (10a) to estimate the new surface temperature of the next iteration can significantly reduce the number of global iterations. They can be defined in two equivalent ways: an H-type convective condition

$$C_H = q_{c,w(\mathrm{CFD})}/(H_r - H_w) \tag{10b}$$

or, alternatively, a T-type convective condition

$$C_T = q_{c,w(\mathrm{CFD})}/(T_r - T_w) \tag{10c}$$

can be used. Here, C_H and C_T are the convective heat-transfer coefficients, H_r and H_w are the total recovery enthalpy and the enthalpy at the surface, respectively, and T_r and T_w are the recovery temperature and surface temperature, respectively. The recovery temperature is defined as

$$T_r = \frac{C_{pe}}{C_{pw}} T_e + \frac{0.5U_e^2}{C_{pw}} \tag{10d}$$

Using these definitions in Eq. (10a), the surface temperature for the next iteration can be obtained from the following expressions:

$$C_H(H_r - H_w) + q_{\mathrm{rad}} = \rho v h_w - J_v h_s + \varepsilon\sigma T_w^4 + q_{\mathrm{cond}} \tag{10e}$$

or

$$C_T(T_r - T_w) + q_{\mathrm{rad}} = \rho v h_w - J_v h_s + \varepsilon\sigma T_w^4 + q_{\mathrm{cond}} \tag{10f}$$

The convective conditions discussed above are only used for estimating the new surface temperature of the next iteration so that rapid convergence is obtained. Once the solution is obtained, the convective heat flux is exactly equal to that computed from the Navier-Stokes solver. Thus, the accuracy of solution is independent of the definitions used in Eqs. (10b–10d). Based on the cases we have examined, it was found that the T-type convective condition (10f) was as effective as the H-type convective condition (10e). Total enthalpy is a function of temperature, pressure, and species concentrations. Thus, an H-type condition must be solved with flow properties provided from CFD calculations to obtain the surface temperature. A T-type condition appears to be more attractive for the cases with significant in-depth conduction, because it is not necessary to pass a large database of flow properties from the CFD code to the CSM code.

This procedure calculates both chemical-equilibrium and nonequilibrium surface conditions. The partial derivative terms in Eqs. (1–10) are discretized using a second-order finite-difference method. For chemical-nonequilibrium surface conditions, the surface temperature is calculated from Eqs. (10a–10f) using the Newton-Raphson method. The surface ablation rate is calculated from Eq. (3) with available correlations or kinetic theory, and the surface species concentrations are calculated from Eq. (1) and available surface-kinetics models or frozen chemistry. For chemical-equilibrium surface conditions, the surface temperature is obtained from Eqs. (10a–10f) using the Newton-Raphson method. The surface ablation rate is calculated from Eq. (9), with the value of B' at the given surface temperature and pressure obtained from a precalculated $B'(T_w, P_w)$ table using the ACE (aerotherm chemical equilibrium) program[17] and the bicubic spline routines of the International Mathematical and Statistical Library (IMSL).[20] The species concentrations are obtained from Eq. (4) and the equilibrium relations of ACE. The thermodynamic properties are based on the JANAF correlations.[21]

In the Navier-Stokes code, the surface temperature, species concentrations, and velocities are updated by the CST procedure as the residual of Navier-Stokes calculations reaches a certain preset value. Otherwise, the surface conditions are kept unchanged. This iteration process will continue until both the flowfield and surface properties reach steady-state conditions. The best timing for updating the surface conditions is code-dependent. Based on our experience, inappropriate timing may drive the iteration in the wrong direction. So far, no attempt has been made to optimize this global iteration process between CST and CFD codes. A relaxation factor less than one is usually imposed on updating the new surface temperature in Eq. (2) to avoid the abrupt change of surface blowing velocity because the ablation rate is essentially an exponential

function of temperature. The total computational time for reaching a steady-state solution depends on the number of iterations required for the CFD calculations to reach the preset residual after the surface conditions are updated by the CST code, and on the computational time required for each iteration.

Gas and Surface Models for the Test Case

The flowfield calculations for the test case were performed using GASP. This is a general-purpose code and requires a small amount of work, compared with other available codes, to implement new species and chemical reactions. The GASP code was run in the implicit mode, with the approximate factorization algorithm, Van Leer flux vector splitting method, upwind-biased third-order scheme, finite-rate chemistry, and full Navier-Stokes formulation. Since GASP has no capability of computing flow with unequal diffusion coefficients, the equation with equal diffusion coefficients [Eq. (5)] was applied in the surface chemistry computation. The gas phase is modeled with 10 species (N_2, O_2, NO, N, O, C, C_2, C_3, CO_2, and CO) and 14 chemical reactions. The gas reactions are as follows:

$$CO_2 + M_1 \rightleftharpoons CO + O + M_1$$

$$CO + M_2 \rightleftharpoons C + O + M_2$$

$$N_2 + M_3 \rightleftharpoons 2N + M_3$$

$$O_2 + M_4 \rightleftharpoons 2O + M_4$$

$$NO + M_5 \rightleftharpoons N + O + M_5$$

$$C_2 + M_6 \rightleftharpoons 2C + M_6$$

$$C_3 + M_7 \rightleftharpoons C + C_2 + M_7$$

$$CO + N \rightleftharpoons NO + C$$

$$CO + CO \rightleftharpoons CO_2 + C$$

$$CO + O \rightleftharpoons O_2 + C$$

$$N_2 + O \rightleftharpoons NO + N$$

$$NO + CO \rightleftharpoons CO_2 + N$$

$$NO + O \rightleftharpoons O_2 + N$$

$$CO_2 + O \rightleftharpoons O_2 + CO$$

Very few sources provide the gas reaction-rate data for typical TPS ablators in air or CO_2 environments. The reaction-rate data adopted in this study are from the work of Bhutta and Lewis.[10] This is the only consistent source presently available. The accuracy of these reaction rates is unknown. Studies conducted to develop surface chemical reaction-rate data for TPS materials are rare, and most of them have concentrated on the surface catalysis effect for nonablating surfaces.[2–4] Therefore, two extreme surface conditions were examined in this paper. They are a chemically frozen surface and a chemically equilibrated surface. If the surface is frozen, the source term in the species conservation equation (1) is equal to zero, and if the surface is also nonablating ($J_v = \rho v = 0$), the species equation is then reduced to that of a noncatalytic surface. For chemically frozen surfaces, the net ablation rate J_v is calculated using the following expression[15]:

$$J_v = \frac{0.8 m \sigma_v P_v}{(2\pi m k T_w)^{0.5}} \tag{11}$$

Here, the saturated vapor pressure P_v of surface material is characterized by the preexponential factor and the activation energy for evaporation. Additionally, in the frozen-surface calculations, it is assumed that the gas-phase carbon species at the surface are represented by C_3. In reality, carbon may not ablate predominantly as C_3 except in an inert environment or for strong blowing. For fully

Table 1 Freestream conditions of a proposed hypersonic test vehicle

Cond.	Time, s	Altitude, km	Velocity, km/s	Pressure, atm	Temperature, K
1	287	30.48	4.889	0.0110	227
2[a]	300	24.38	4.572	0.0276	221
3	315	28.34	4.362	0.0155	225
4	323	30.48	4.304	0.0110	227

[a]Peak heating point.

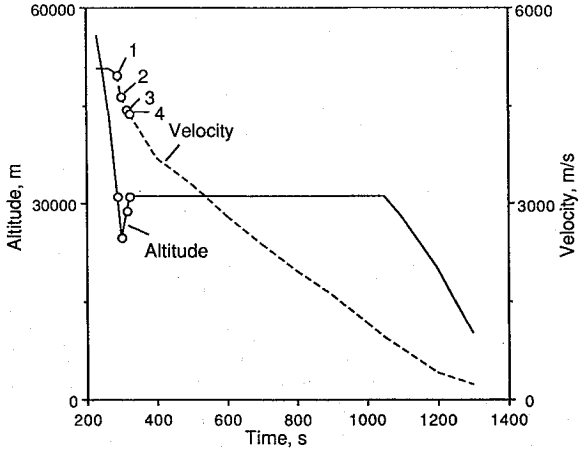

Fig. 3 Trajectory for proposed hypersonic test vehicle.

equilibrium surfaces, the net ablation rate J_v is calculated using a $B'(T_w, P_w)$ table generated by the ACE code with graphite and 10 gas species. The surface pressure P_w of the pre-calculated B' curve is in the range from 0.5 to 13 atm. In the test cases, the radiative equilibrium boundary condition is used; that is, in-depth heat conduction is assumed to be zero, and the convective heat flux is balanced by the energy radiated from the surface.

Results and Discussion

The trajectory for a proposed hypersonic test vehicle used as the test case is shown in Fig. 3. This vehicle has a graphite nosetip with a radius R_n of 0.0176 m, and a cone half angle of 6.5 deg. Calculations were performed using the freestream conditions near the peak heating point (symbols), and are listed in Table 1. Solutions with various surface boundary conditions are presented in this paper to examine their effects on the predictions of flow structure and surface conditions. The first set of solutions presented in this section were calculated with boundary conditions for a nonablating surface. The effect of chemical reaction on the flow structure and surface radiative equilibrium temperature is examined. The second set of solutions were obtained using an isothermal surface condition with various surface blowing rates. The detailed flow structure and surface heating distributions for various surface blowing rates are discussed. The third set of solutions were obtained with the complete conditions of mass and energy balance for an ablating graphite surface. The effect of surface chemistry on the predictions of the surface ablation rate was examined, and the solutions from GASP with complete boundary conditions were compared with ASCC solutions at four different trajectory points.

Figure 4a shows the predicted surface temperature profiles over the spherical nosetip at the peak heating point (case 2 in Table 1). For this nonablating case, the surface emissivity was assumed to be 0.85. Two extremes were examined: the dashed line is the solution for flow with equilibrium gas and surface chemistry, and the solid line is the solution for flow with finite-rate gas chemistry and frozen surface chemistry. To examine the consistency of GASP, a noncatalytic surface solution computed by the Gauss-Siedel implicit aerothermodynamic Navier-Stokes code with thermochemical surface conditions (GIANTS)[6] is also presented (dashed line). The GIANTS code is a two-dimensional axisymmetric multicomponent full Navier-Stokes solver with two-temperature model. The maximum difference between two solutions is less than 3%. In addition, the comparison between GASP solutions with surface catalysis and

shock-tunnel data was studied in Ref. 22. Also as seen in Fig. 4a, the predicted surface temperature with fully equilibrium chemistry is substantially higher than that with finite-rate gas chemistry and frozen surface chemistry. The difference between the two solutions at the stagnation point is about 400 K. This trend is similar to that between the fully catalytic and noncatalytic surfaces.[5,6] The predictions suggest that the surface heating rate is sensitive to the chemistry model. Without reliable chemical reaction-rate data for both gas and surface reactions, the accurate prediction of surface heating is unlikely.

The temperature profiles and species concentration distributions (O, N, and NO) along the stagnation streamline are shown in Figs. 4b and 4c, respectively, for the nonablating calculation. The solutions indicate that the temperature for finite-rate-chemistry flow at the shock is around 2000 K higher than that of fully equilibrium flow. The temperature for finite-rate-chemistry flow remains higher than that of fully equilibrium flow in the outer third of the shock layer. For a fully equilibrium gas chemistry condition, some of the thermal energy is converted to chemical energy instantaneously as the flow crosses the shock. For finite-rate gas chemistry, the flow remains chemically frozen at the shock and gradually approaches the equilibrium condition if the shock-standoff distance is large enough (Fig. 4c). The predicted species concentrations in the region near the surface are quite different between these two calculations. This is mainly a result of the difference in the surface-chemistry models, and strongly affects the convective heating to the surface.

The effect of surface blowing on the flowfield and surface heating is shown in Figs. 5a to 5c for the second test case. The stream conditions are those at the peak heating point (case 2 in Table 1). The surface is assumed to be isothermal (3000 K) and with frozen surface chemistry. The computations were performed using finite-rate gas chemistry. The air blowing-rate ratios m_b, which extend from the stagnation point to 0.95 cm downstream, were set to 0.005, 0.05, and 0.5, respectively, and over the rest of the body, the surface blowing rates were set to zero. Even with the nondimensional surface blowing rates as high as 0.5, no computational difficulty was encountered in the GASP code. The temperature profiles and species-concentration distributions along the stagnation streamline for various surface blowing rates are presented in Figs. 5a and 5b, respectively. As expected, the shock-standoff distance increases as the blowing rate increases. For $m_b = 0$ and $m_b = 0.005$, the standoff distances are about the same. The standoff distance with $m_b = 0.5$ is about two times as large as that with $m_b = 0$. At low blowing rates ($m_b = 0.005$ and 0.05), the temperature and species gradients near the surface are reduced by the surface blowing, and the global structure of the shock layer remains essentially unchanged. The predictions also indicate that a relatively cold region with fairly uniform properties is formed near the surface for the very strong blowing rate ($m_b = 0.5$). The formation of this cold sublayer is similar to the presence of a virtual surface located at a certain distance from the real surface, since the surface blowing is large enough to displace the boundary layer away from the true solid surface. The temperature and species concentration profiles between the virtual surface and shock are still similar to those without surface blowing between the true surface and shock. As indicated from the solutions, an adaptive grid may be necessary to precisely determine the locations of the virtual surface and shock. The reduction of surface heating with increased mass injection for various surface blowing rates is shown in Fig. 5c. For $m_b = 0.5$, the surface convective heat flux remains completely blocked over the entire region where $m_b = 0$.

The solutions coupled with complete ablating-surface boundary conditions are presented in Figs. 6 and 7. The predicted surface temperature profiles over the nosetip are shown in Fig. 6a. The solid and dashed lines represent the surface temperature distributions for ablating and nonablating surface conditions, respectively. The calculations were conducted with the GASP code with finite-rate gas chemistry and equilibrium surface chemistry. Over an ablating surface, part of the incident heat flux to the surface contributes to vaporizing the graphite, and part of the incoming flow energy is blocked by the vaporized graphite through chemical reactions or change of internal energy. Hence, the predicted surface temperature is lower than

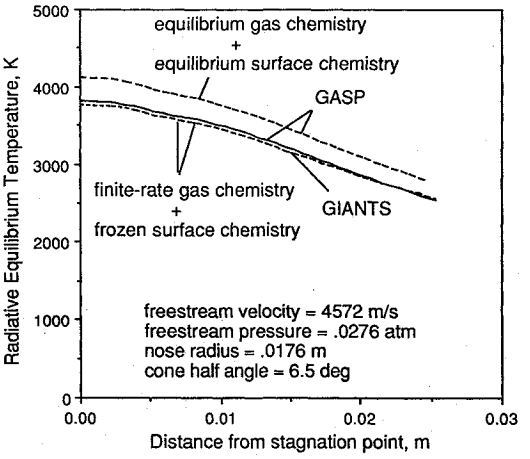

a)

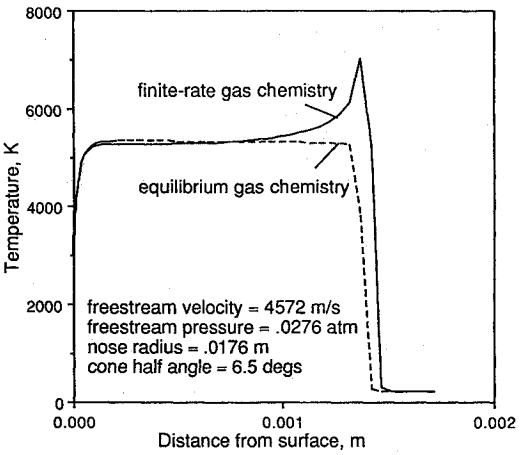

b)

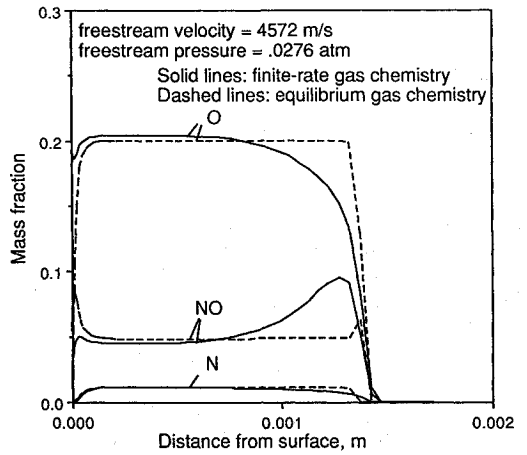

c)

Fig. 4 a) Effect of gas chemistry on surface temperature (nonablating surface), b) temperature profiles along stagnation streamline (nonablating surface), and c) species concentrations along stagnation streamline (nonablating surface).

that in the nonablating case. The steady-state surface temperature computed by the ASCC code (symbols) without in-depth conduction agrees with that of GASP for equilibrium surface chemistry. Surface ablation rates predicted by the GASP and ASCC codes are shown in Fig. 6b. Ablation rates at the stagnation point predicted by GASP with equilibrium surface chemistry (solid line) are about 55% higher than that of GASP with frozen surface chemistry (dashed line). This again illustrates that the predictions of surface ablation and heating

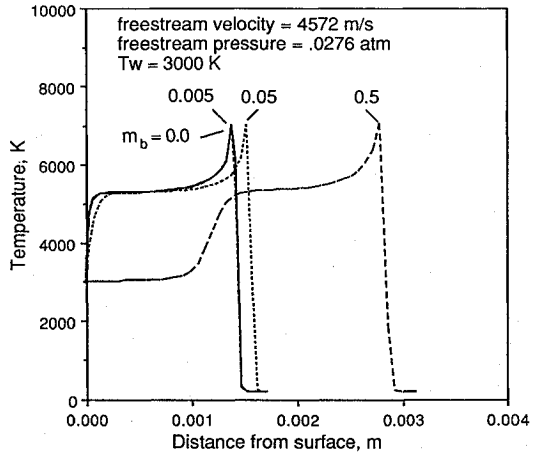

a)

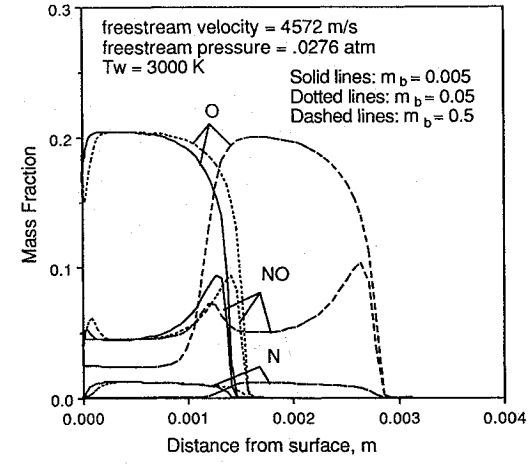

b)

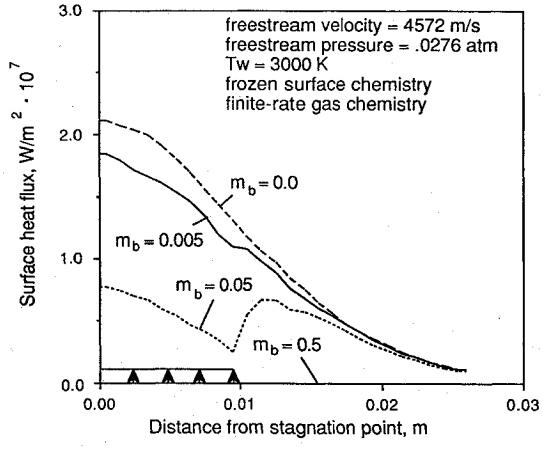

c)

Fig. 5 a) Effect of surface blowing on temperature profiles along stagnation streamline, b) effect of surface blowing on species concentrations along stagnation streamline, and c) effect of surface blowing on surface heating.

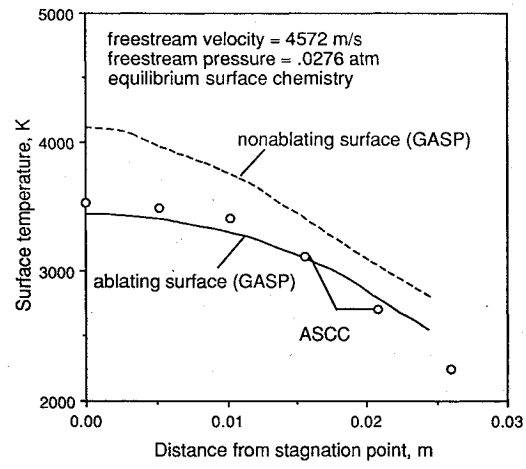

a)

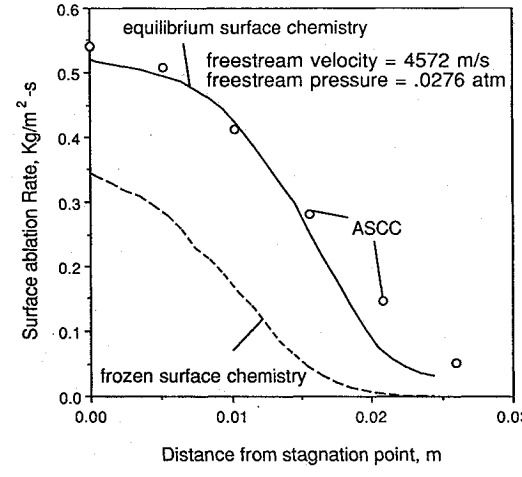

b)

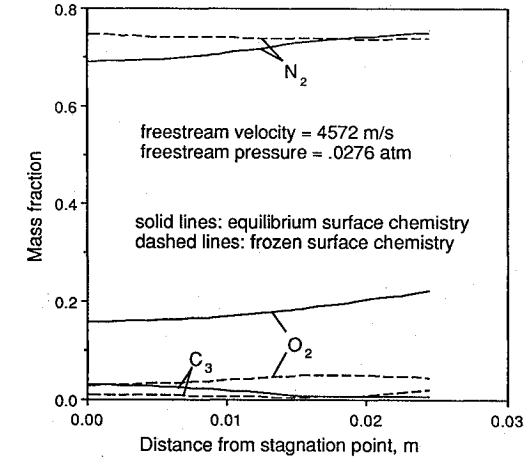

c)

Fig. 6 a) Effect of surface ablation on surface temperature profiles, b) surface ablation rates at peak heating point, and c) effect of surface chemistry on species concentration profiles along surface.

rates for this test case are very sensitive to the surface chemistry. Surface reaction-rate data are essential for accurately predicting the surface heating and ablation. As compared to GASP using equilibrium surface chemistry, the ASCC code predicted a slightly higher steady-state ablation rate. Figure 6c shows the species concentration (N_2, O_2, and C_3) surface distribution that is predicted by GASP using equilibrium (solid lines) and frozen (dashed lines) surface chemistry models. This figure clearly indicates that a significant difference appears between the predictions of two surface models, which results in a 55% difference in the surface ablation rate.

The stagnation-point ablation rates at various trajectory points (cases 1–4 in Table 1) computed using the GASP and ASCC codes are presented in Fig. 7. In the time-dependent ASCC predictions, the solutions with and without in-depth conduction are presented, respectively. The surface ablation rates predicted with in-depth conduction are lower than those without in-depth conduction. In the GASP calculations, each point was treated as an isolated steady-state case without conduction loss into the wall or shape change.

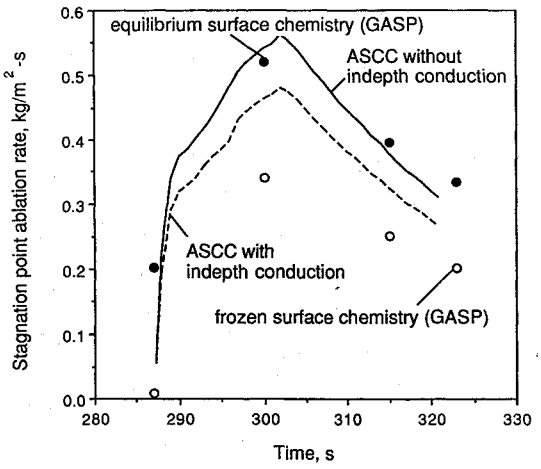

Fig. 7 Stagnation-point ablation rates at various trajectory times.

The time-dependent ASCC predictions without in-depth conduction are generally consistent with the GASP solutions using equilibrium surface chemistry, since without in-depth conduction each trajectory point is an isolated steady-state case. The GASP solutions with the frozen-surface are far smaller than those with the equilibrium-surface model.

Conclusions

The general surface boundary conditions with mass and energy balances of chemically equilibriated or nonequilibriated gas adjacent to an ablating surface were derived. A computer procedure based on these surface conditions was developed and interfaced with GASP. A test case with a proposed hypersonic test-vehicle configuration and associated freestream conditions was developed. The predictions of GASP with chemically equilibrated ablating surface conditions were consistent with those of the ASC code. Solutions with various surface boundary conditions were obtained to study the effects of gas and surface chemistry on surface heating and ablation rate. The solutions indicate that the predictions of surface temperature and ablation rate are very sensitive to the gas as well as surface chemistry models for the test case. However, a reliable chemical reaction-rate database for both gas and surface reactions over the TPS ablators is not available. The calculations using an equilibrium surface chemistry model can provide information for the most conservative TPS design, and the study of detailed surface thermal chemistry over ablating or nonablating materials may help in computing more accurate surface heating values and reducing the thickness of the TPS.

Acknowledgments

Support for Y.K.C. by NASA (Grant NCC2-462) is gratefully acknowledged. The authors greatly appreciate the input from discussion with Dr. F. S. Milos at NASA Ames Research Center.

References

[1]Milos, F. S., and Rasky, D. J., "A Review of Numerical Procedures for Computational Surface Thermochemistry," AIAA Paper 92-2944, July 1992.

[2]Kolodziej, P., and Stewart, D. A., "Nitrogen Recombination on High-Temperature Reusable Surface Insulation and the Analysis of Its Effect on Surface Catalysis," AIAA Paper 87-1637, June 1987.

[3]Zoby, E. V., Gupta, R. N., and Simmonds, A. L., "Temperature Dependent Reaction Rate Expressions for Oxygen Recombination," AIAA Paper 84-0224, Jan. 1984.

[4]Scott, C. D., "Catalytic Recombination of Nitrogen and Oxygen on High-Temperature Reusable Surface Insulation," AIAA Paper 76-444, July 1980.

[5]Chen, Y.-K., Henline, W. D., Stewart, D. A., and Candler, G. V., "Navier-Stokes Solutions with Surface Catalysis for Martian Atmospheric Entry," *Journal of Spacecraft and Rockets*, Vol. 30, No. 1, 1993, pp. 32–42.

[6]Chen, Y.-K., and Henline, W. D., "Analysis of Hypersonic Arcjet Flow Fields and Surface Heating of Blunt Bodies," AIAA Paper 93-0272, Jan. 1993.

[7]Bartlett, E. P., and Kendall, R. M., "An Analysis of the Coupled Chemically Reacting Boundary Layer and Charring Ablator, Part III: Nonsimilar Solution of the Multicomponent Laminar Boundary Layer by an Integral Matrix Method," NASA CR-1062, June 1968.

[8]Moss, J. N., Anderson, E. C., and Bolz, C. W., Jr., "Aerothermal Environment for Jupiter Entry Probes," edited by Allie M. Smith, *Progress in Astronautics and Aeronautics*, Vol. 56, AIAA, New York, 1976, pp. 333–354.

[9]Nicolet, W. E., Walterland, L. R., and Kendall, R. M., "Methods for Predicting Radiation-Coupled Flowfields About Planetary Entry Probes," edited by Leory S. Fletcher, *Progress in Astronautics and Aeronautics*, Vol. 59, AIAA, New York, 1978, pp. 120–136.

[10]Bhutta, B. A., and Lewis, C. H., "A New Technique for Low-To-High Altitude Predictions of Ablative Hypersonic Flowfields," *Journal of Spacecraft and Rockets*, Vol. 29, No. 1, 1992, pp. 35–50.

[11]Conti, R. J., MacCormack, R. W., Groener, L. S., and Fryer, J. M., "Practical Navier-Stokes Computation of Axisymmetric Reentry Flowfields with Coupled Ablation and Shape Change," AIAA Paper 92-0752, Jan. 1992.

[12]Walters, R. W., Cinnella, P., Slack, D. C., and Halt, D., "Characteristic-Based Algorithms for Flows in Thermo-chemical Nonequilibrium," AIAA Paper 90-0393, Jan. 1990.

[13]King, H. H. C., Muramoto, K. K., Murray, A. L., and Pronchick, S. W., "ABRES Shape Change Code (ASCC 86): Technical Report and User's Manual," Report FR-88-24/ATD, Acurex Corp., Mountain View, CA, Dec. 1986.

[14]Dahm, T. J., Cooper, L., Rafinejad, D., Youngblood, S. B., and Kelly, J. T., "Passive Nosetip Technology (PANTII) Program, Vol. 1, Inviscid Flow and Heat Transfer Modeling for Reentry Vehicle Nosetips," Report SAMSO-TR-77-11, Acurex Corp., Mountain View, CA, Oct. 1976.

[15]Hassanein, A. M., Kulcinski, G. L., and Wolfer, W. G., "Vaporization and Melting of Materials in Fusion Devices," *Journal of Nuclear Materials*, Vols. 103 & 104, Mar. 1981, pp. 321–326.

[16]Risch, T. K., and Laub, B., "General Model for Thermochemical Ablation into a Vacuum," *Journal of Thermophysics*, Vol. 4, No. 3, 1990, pp. 278–284.

[17]Anon., "User's Manual: Aerotherm Chemical Equilibrium Computer Program," Report UM-81-11/ATD, Acurex Corp., Mountain View, CA, Aug. 1981.

[18]Henline, W. D., and Tauber, M. E., "Trajectory-Based Heating Analysis for the ESA/Rosetta Earth Return Vehicle," AIAA Paper 93-0269, Jan. 1993.

[19]Henline, W. D., Chen, Y.-K., Palmer, G. E., and Stewart, D. A., "Trajectory Based, 3-Dimensional Heating and Ablation Calculations for the Apollo Lunar/Earth Return Capsule," AIAA Paper 93-2788, July 1993.

[20]Anon., *User's Manual: Fortran Subroutines for Mathematical Applications*, MATH/LIBRARY, IMSL, Version 2.0, Sept. 1991.

[21]Anon., *JANAF Thermochemical Tables*, The Thermal Research Laboratory, Dow Chemical Company, Midland, MI, July 1964.

[22]Chen, Y.-K., and Henline, W. D., "Three-Dimensional Nonequilibrium Hypersonic Flow and Heating Analysis of a 140-deg Blunt Body in NASA-Ames 42-in. Shock Tunnel," AIAA/ASME 6th Joint Thermophysics and Heat Transfer Conference, June 1994.